ACS APPLIED MATERIALS & INTERFACES

Research Article

Cite This: ACS Appl. Mater. Interfaces 2018, 10, 6730−6736

www.acsami.org

Single-Crystal Graphene-Directed van der Waals Epitaxial Resistive Switching

Xin Sun,*[,†] Zonghuan Lu,[†] Zhizhong Chen,[‡] Yiping Wang,[‡] Jian Shi,[‡] Morris Washington,[†] and Toh-Ming Lu[†]

[†]Department of Physics, Applied Physics and Astronomy, and Center for Materials, Devices and Integrated Systems, and [‡]Department of Materials Science and Engineering, Rensselaer Polytechnic Institute, Troy, New York 12180, United States

Supporting Information

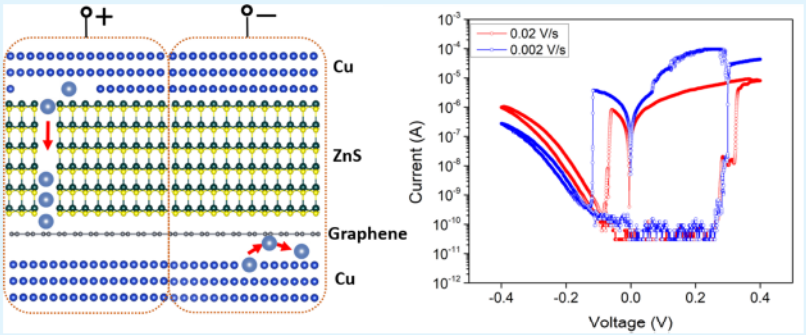

ABSTRACT: Graphene has been broadcasted as a promising choice of electrode and substrate for flexible electronics. To be truly useful in this regime, graphene has to prove its capability in ordering the growth of overlayers at an atomic scale, commonly known as epitaxy. Meanwhile, graphene as a diffusion barrier against atoms and ions has been shown in some metal−graphene−dielectric configurations for integrated circuits. Guided by these two points, this work explores a new direction of using graphene as a bifunctional material in an electrochemical metallization memory, where graphene is shown to (i) order the growth of a low-ionicity semiconductor ZnS single-crystalline film and (ii) regulate the ion migration in the resistive switching device made of Cu/ZnS/graphene/Cu structures. The ZnS film is confirmed to be van der Waals epitaxially grown on single-crystal graphene with X-ray structural analysis and Raman spectroscopy. Charge transport studies with controlled kinetic parameters reveal superior ion regulating characteristic of graphene in this ZnS-based resistive switching device. The demonstration of the first graphene-directed epitaxial wide band gap semiconductor resistive switching suggests a possible and promising route toward flexible memristors.

KEYWORDS: *graphene, van der Waals epitaxy, ZnS, electrochemical metallization memories, ion migration, resistive switching*

INTRODUCTION

Graphene has long been regarded as the cornerstone for future flexible electronics because of its extraordinary properties of transferability, electrical conductivity, transparency, lightweight, ductility, chemical inertness, and so forth.[1] In addition, graphene offers an important attractiveness which might have been understated in the past, that is, the template function to order the atomic arrangement of overlayers grown on top of a single-crystalline graphene substrate, which could be categorized as van der Waals epitaxy (vdWE). Recently, van der Waals heterojunctions of 2D transition metal dichalcogenides (TMD) on graphene have become an active research field, and the progress in this field deserves credit.[2] However, from the perspective of practical applications, vdWE of conventional 3D semiconductors, such as II−VI and III−V compounds, on graphene may carry more significance because these semiconductors are the proven working horses in optoelectronics and microelectronics. vdWE of 3D semiconductors on graphene, typically via vapor-phase epitaxy, is more challenging than those TMD−graphene junctions made by exfoliation, as the pristine graphene surface is hard to wet because of the lack of dangling bonds and nucleation sites. Defected graphene, either transferred or intentionally induced, may relieve the wetting issue but at the price of crystal quality of overlayers.[3−5]

Resistive memory is a simple two-terminal device relying on the resistive switching phenomenon that can virtually be realized in all insulators and semiconductors. Among various kinds of resistive memories, the electrochemical metallization (ECM) cell, also known as the conductive-bridge memory, is a popular choice that memorizes a state based on the migration of metal cations. ECM consists of an active metal anode, such as Cu, a solid electrolyte, such as oxides or chalcogenides, and an inert metal cathode, such as Pt.[6−8] With a positive bias at the anode, cations of the active metal are formed at the anode

Received: December 3, 2017
Accepted: January 25, 2018
Published: January 25, 2018

DOI: 10.1021/acsami.7b18385
ACS Appl. Mater. Interfaces 2018, 10, 6730−6736

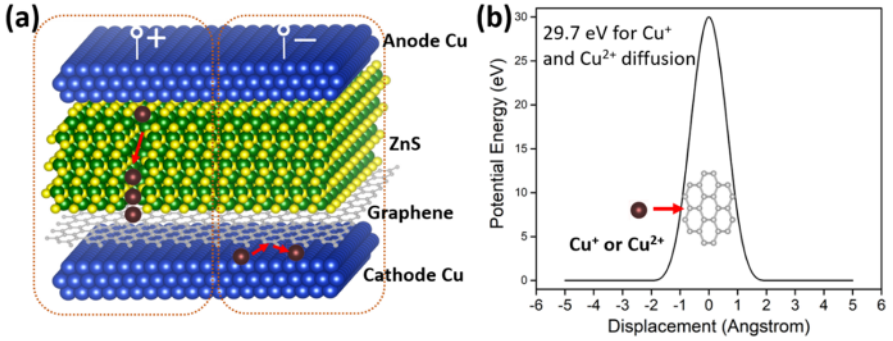

Figure 1. (a) Schematic side view of the Cu/ZnS/graphene/Cu ECM memory; under a positive bias, Cu ions supplied from the anode (top) electrode swimming to the cathode (bottom) electrode and forming a CF; under a negative bias, Cu ions, if generated at the bottom Cu electrode, bouncing back from the graphene barrier. (b) Potential barrier for the diffusion of Cu ions through a perfect monolayer graphene (data replotted from a DFT calculation[11]).

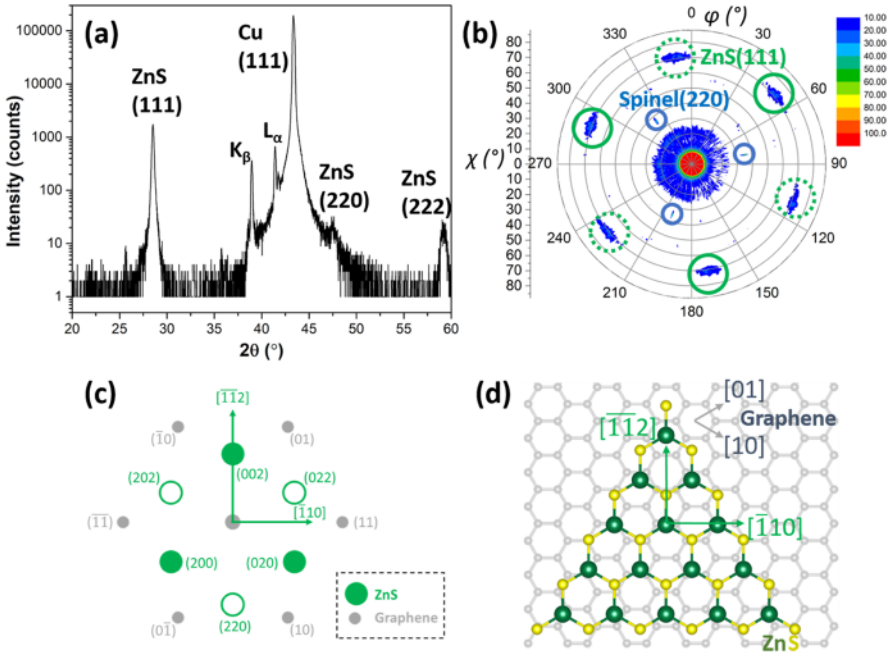

Figure 2. (a) XRD ω–2θ pattern of a ZnS(111)/graphene/Cu(111)/spinel(111) film stack; peaks at $2\theta = 38.9°$ and 41.4° result from Cu Kβ and W Lα X-ray lines which are the contamination lines in the X-ray source; these peaks can thus be ignored. (b) ZnS(111) X-ray pole figure: green circled: ZnS poles; blue circled: spinel poles. (c) Reciprocal space lattice overlay of ZnS(111) on graphene. (d) Real space atomic model of ZnS(111) on graphene.

interface and transported through the electrolyte to the cathode interface where they grow into conductive filaments (CFs). Once formed, CFs bridge the cathode and anode and result in a dramatic decrease of resistance, corresponding to an operation of SET, and the memory becomes ON. When the bias polarity is reversed to a certain degree, CFs rupture, and the memory returns to a high-resistance state, or simply OFF, corresponding to an operation of RESET. In ECM memories, at least one inert metal is usually used in that the inert metal is not expected to form CF under a reversed bias. Otherwise, the device may encounter issues to switch off.

Graphene has been demonstrated as an excellent diffusion barrier against both Cu atoms and ions in studies of Cu/graphene/SiO_x stacks for microelectronics.[9,10] This leads us to conceive a study bringing graphene together with ECM memories, specifically making use of graphene to regulate the migration of Cu ions. In brief, we demonstrate a bipolar ECM memory using Cu as an active electrode, a vdWE ZnS thin film as a solid electrolyte, and epitaxial graphene/Cu as an inert electrode. Figure 1a shows the schematic view of this device. Compared to commonly used ECM memories, this design distinguishes itself by utilizing graphene/Cu in place of a noble metal as the inert electrode. Under a positive bias, Cu ions originating from the graphene-free Cu electrode are expected to perform their normal duties by migrating and forming CFs. However, the story in this memory becomes different when the bias polarity is reversed. Under a negative bias, it is likely that the epitaxial graphene-covered Cu electrode will not form mobile Cu ions in the first place because of the protection by graphene. Even if the mobile ions are indeed formed between graphene and the bottom Cu electrode, they will be bouncing back when attempting to pass through the safety net set by graphene. This anticipation can be backed up by a density function theory (DFT) calculation by Zhao et al.[11] According to the DFT calculation, shown in Figure 1b, the diffusion potential barrier that a perfect monolayer graphene imposes on

DOI: 10.1021/acsami.7b18385
ACS Appl. Mater. Interfaces 2018, 10, 6730–6736

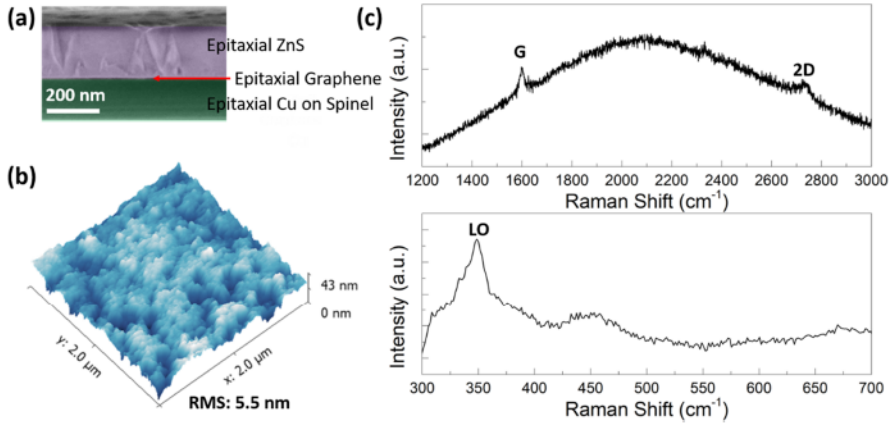

Figure 3. (a) Cross-sectional SEM image and (b) AFM image of a ZnS(111) film grown on the graphene/Cu(111)/spinel(111) substrate. (c) Raman spectra of the ZnS(111) film grown on the graphene/Cu(111)/spinel(111) substrate; upper: graphene region; bottom: ZnS region.

Cu^+ or Cu^{2+} is as large as 29.7 eV (E_b). This means at room temperature, the probability, $P = \exp\left(-\frac{E_b}{k_B T}\right)$, for a Cu ion to sneak through the graphene net is tiny. In fact, this knowledge of graphene's superior blocking ability should not be striking if one refers to the function of graphite in lithium-ion batteries, where the smallest metal ion could not pass the screening of a graphene sheet.

Another motive to use epitaxial graphene/Cu as the key component for this ECM memory is the multifold benefits coming from graphene/Cu. First, graphene grown on Cu catalysis substrates is probably the most common way to synthesize graphene at a large scale.[12,13] Hence, producing graphene/Cu heterostructures should not be a challenging task from the technology point of view. Second, unlike many other graphene-based devices,[14,15] resistive memories included,[16,17] the graphene for this use does not have to undergo any transfer process which would inevitably deteriorate the quality of graphene.[18,19] Third, graphene is challenging to wet because of its low surface energy, and it is thus challenging for a high-quality film to grow on graphene. However, with Cu underneath graphene, the potential barrier for films to nucleate on graphene can be relieved, as Cu is speculated to enhance the nucleation on graphene.[20] Fourth, films grown on graphene will follow the vdWE mechanism, and thus, the growth will inherit the benefits from vdWE, such as the loose constraint on a lattice mismatch aspect.[21] As for choosing ZnS as the electrolyte, which in fact is not unusual in the literature,[22,23] the main reason is that this material is more likely to be vdWE grown on graphene compared to oxide insulators. Furthermore, the wide band gap and optical transparency of ZnS allow the underlying graphene to be characterized with direct evidence using "see-through" Raman spectroscopy.

RESULTS AND DISCUSSION

The device fabrication in this work consisted of three steps. First, single-crystalline graphene was grown on Cu(111)/spinel(111) substrates using a chemical vapor deposition method.[24] Second, epitaxial ZnS(111) films were grown on graphene/Cu(111)/spinel(111) substrates using a thermal evaporation method. The substrate temperature, deposition rate, and film thickness were 150 °C, 3 Å/s, and 200 nm, respectively. Last, 150 nm thick Cu was deposited as the top electrode using the same evaporation system with a shadow mask (opening of 0.5 mm in diameter), but the substrate was not intentionally heated. More information regarding the evaporation process can be found elsewhere.[5]

Figure 2a shows the X-ray diffraction (XRD) ω–2θ pattern of a ZnS film grown on graphene/Cu(111)/spinel(111). The film is found to be in a zinc-blende phase (space group 216, $F\bar{4}3m$) with a dominating (111) out-of-plane orientation. There is a tiny ZnS(220) diffraction present with an extremely low intensity in comparison with that of the ZnS (111) peak, and the contribution is negligible. All other peaks between 35° and 45° in the 2θ scan originate from the (111) diffraction (Cu Kα line) and the associated contamination lines (Cu Kβ and W Lα) of the single-crystal Cu film underneath the graphene. To reveal the texture of the film, a ZnS(111) X-ray pole figure was collected using a fixed Bragg angle (2θ) at 28.5°, polar angle (χ) from 0 to 88° (step size: 2°), and azimuthal angle (φ) from 0 to 359° (step size: 1°). The ZnS(111) pole figure in Figure 2b shows six poles at χ of 70.5°, and the poles are 60° apart each other in the azimuthal direction, corresponding to the primary set of three ZnS(111) poles (in solid circles) and a secondary set of three ZnS(111) poles (in dash circles). The pole figure is indicative of the single-crystal nature of the ZnS film with two (111) domains offset by 60° in-plane. In other words, one of the ZnS(111) domains is rotated 60° in-plane and is therefore a twin domain to the other. The 60° in-plane twinning of cubic (111) films is a common phenomenon reported in the literature.[4,25] Although the ZnS film has a preferred in-plane orientation, note that the dispersion of the ZnS(111) poles is relatively large, suggesting the existence of small-angle grain boundaries in the film. Nevertheless, the ZnS film is indeed in an epitaxial form. The epitaxial alignment between ZnS(111) and graphene can be deduced with the aid of those three spinel (220) poles at χ of 35°. Their appearance in the pole figure is due to the close 2θ (31.2°) for this diffraction with respect to the preset 2θ for ZnS. It can be seen that there is a 30° rotation between ZnS(111) and spinel (220) poles. According to our previous work, the Cu(111) film is in parallel epitaxy with spinel(111), that is, Cu(111)||spinel(111) and Cu $[\bar{1}10]$||spinel $[\bar{1}10]$.[24] Furthermore, graphene is known to be in parallel epitaxy with the Cu(111) film.[26] Given these relations, the reciprocal space lattice overlay of ZnS(111) on graphene can be constructed as shown in Figure 2c. Figure 2d presents a clearer view of how ZnS(111) aligns on top of graphene using an atomic model in real space. The vdWE alignment between ZnS and graphene can be interpreted as follows; ZnS(111)||graphene and ZnS $[\bar{1}10]$ offset 30° with

DOI: 10.1021/acsami.7b18385
ACS Appl. Mater. Interfaces 2018, 10, 6730–6736

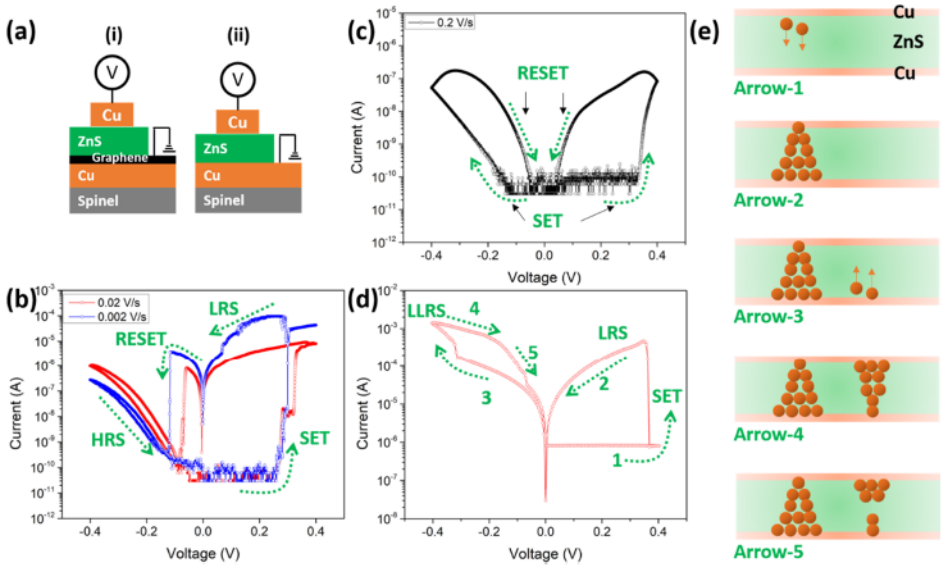

Figure 4. (a) Test structure of the Cu/ZnS/graphene/Cu and Cu/ZnS/Cu ECM memory devices. (b) I–V characteristics of the Cu/ZnS/graphene/Cu ECM memory with scan rates of 0.002 and 0.02 V/s. The top electrode was initially applied with the positive bias voltage, which also applies to all the remaining I–V curves. (c) I–V characteristics of the Cu/ZnS/graphene/Cu ECM memory device with a scan rate of 0.2 V/s. (d) I–V characteristics of the Cu/ZnS/Cu ECM memory device with a scan rate of 0.02 V/s. (e) Schematic illustration of the two-way CF forming in the Cu/ZnS/Cu ECM memory.

respect to graphene [10]. The ZnS(111) twin domain is not shown in Figure 2c or d to avoid complexity.

Figure 3a shows a cross-sectional scanning electron microscopy (SEM) image of the ZnS film. The cross section was created by manual cleaving, which explains why it is not as smooth as those cut by a focus ion beam. However, the film quality can be surely inferred to be high as the film looks like a bulk crystal, and no holes or voids can be found under this magnification. The surface morphology of this film is shown with an atomic force microscopy (AFM) image in Figure 3b, characterized with a root-mean-square roughness of ~5.5 nm. Raman spectroscopy with a 514 nm laser line was used to investigate the ZnS–graphene interface. ZnS is known to have the largest band gap (3.5 eV) in II–VI semiconductor compounds, which allows the 514 nm laser to see through the ZnS film even though it is hundreds of nanometers thick. Figure 3c contains two regions of a Raman spectrum obtained from the ZnS(111)/graphene/Cu(111)/spinel(111) film stack. In the upper portion, the characteristic G and 2D peaks of graphene can be clearly observed, confirming the presence of graphene underneath the ZnS film.[27,28] Note that the relatively small peak profile in this spectrum is caused by the high spectral background resulting from the surface plasmon resonance of Cu and does not imply the low quality of graphene.[24,29,30] In the bottom portion, the first-order longitudinal optical phonon of zinc-blende ZnS is seen around 350 cm^{-1}. The spectrum in Figure 3c is representative of 10 random acquisitions. Thus, it is statistically reliable to assume that the sample is homogeneous everywhere.

The resistive switching of this Cu/ZnS(111)/graphene/Cu(111) device, along with a control device of Cu/ZnS/Cu, was studied by sweeping the bias voltage to 0.4 V in both polarities (0 → 0.4 → 0 → −0.4 → 0). The test structure is shown in Figure 4a. Three scan rates, 0.002, 0.02, and 0.2 V/s, were selected to probe the resistive switching behaviors of the device (i) shown in Figure 4a. For the slowest scan rate of 0.002 V/s, shown in Figure 4b, the current jumps from tens of pA to tens of μA at a bias voltage less than 0.3 V, corresponding to a resistance ratio R_{OFF}/R_{ON} on the order of 10^6. This sudden and drastic change from a high-resistance state (HRS or OFF) to a low-resistance state (LRS or ON) suggests the formation of CFs. As the voltage reverses to the negative polarity, the LRS remains till the voltage approaches −0.1 V where the device is reset to the HRS. After reset, no resistive switching is found from −0.1 to −0.4 V. The high asymmetricity of the I–V behaviors under opposite voltage polarity suggests the effectiveness of graphene in regulating the diffusion of Cu ions generated from the bottom Cu electrode. Specifically, because of the presence of graphene, no CF forms when a negative bias voltage is applied on the top electrode because little Cu ions escape from the bottom Cu electrode into the ZnS matrix. Furthermore, it is worth to mention that the initial bias polarity applied on the top Cu electrode has no effect on the resistive switching behaviors in this ECM memory, which is similar to the observation reported by others.[31] In other words, if the bias on the top electrode is initially swept to the negative end, the device will not be turned on. Only when the bias returns to positive, the ON state can be achieved. In short, the I–V curves are the same no matter which polarity is taken first by the top electrode. This is another piece of evidence that CFs only form from one direction, which is the outcome of ion migration regulating by graphene.

Still, in Figure 4b, an overall similar I–V profile can be found from the moderate scan rate of 0.02 V/s. The main difference between this and the 0.002 V/s scan lies in the magnitude of the resistance (R) in the LRS, with the former about 33 times larger than the latter. The contributing factor to this difference may be the different effective diameter (Φ) of CFs formed. A model for filament growth dynamics can be used to qualitatively explain it.[32,33] In details, the resistance of CFs can be expressed in the following form

$$R = \frac{4\rho l}{\pi \Phi^2} \quad (1)$$

DOI: 10.1021/acsami.7b18385
ACS Appl. Mater. Interfaces 2018, 10, 6730–6736

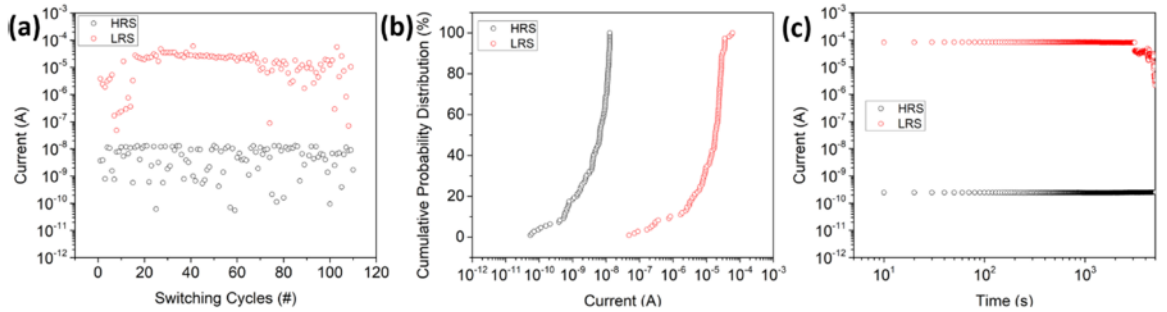

Figure 5. (a) Endurance test of the Cu/ZnS/graphene/Cu ECM memory. The current was measured at 0.2 V. (b) Cumulative probability distribution of the data measured in (a). (c) Retention test of the Cu/ZnS/graphene/Cu ECM memory. The current was measured at 0.15 V.

where ρ is the filament resistivity and l is the filament length (the thickness of the electrolyte film), and Φ is the diameter of the filament and is a function of time and voltage as follows;

$$\frac{d\Phi}{dt} = Ae^{-E_A/kT} \tag{2}$$

and

$$E_A = E_0 - \alpha qV \tag{3}$$

where A is a constant, E_A is the energy barrier for the conductive ion migration, E_0 is the energy barrier at zero bias, α is a constant describing the fraction of the voltage drop, q is the charge, V is the applied voltage, and T is the temperature. Apparently, Φ is time-dependent. According to eq 2, the Φ for the 0.002 V/s scan rate should be 10 times as large as that for 0.02 V/s. However, the actual Φ ratio is ~5.7, according to eq 1 and the resistance ratio shown in Figure 4b. This discrepancy may be related to the complexity of a resistive switching process which by far is not completely understood yet. The model here just qualitatively explains the time factor in filament growth.

The scan rate dependence of resistance is more profound for the scan rate of 0.2 V/s. The $I-V$ curve for this scan rate can be found in Figure 4c. First, the resistance at the LRS for this scan rate is higher compared to those of the other two scan rates, indicating a narrower CF, which is consistent with the argument of time-dependent filament growth. Second, unlike the bipolar switching $I-V$ in Figure 4b, the resistive switching for the 0.2 V/s scan rate appears to be unipolar. This agrees with the assessment of a narrow CF which is unstable and easy to rupture. Third, the $I-V$ profile of this scan rate is not very asymmetric as those in Figure 4b, and the hysteresis shows up in both voltage polarities. This implies that the CF can be formed in both the directions. This appears to be contradicting with the ion regulating role assigned to graphene. To explain it, we propose that the Cu source for forming CFs at this scan rate is from within the ZnS film. Specifically, there could be a small amount of Cu diffusing into the ZnS film when the top Cu electrode was deposited, given the large diffusion coefficients of Cu in II–VI compounds.[34] It is these Cu ions, instead of the Cu ions from electrodes, that respond fast to the fast voltage sweeping. This explanation can also be used to interpret the different turn-on voltages (0.3 and −0.1 V) under different polarities shown in Figure 4c. Because the Cu impurities are more localized around the top electrode, under a positive bias voltage on the top electrode, these Cu ions take a longer time/larger voltage (0.3 V) to reach the bottom electrode to complete the CF growth. For the same reason, the CF forms at a smaller voltage (−0.1 V) the other way.

The $I-V$ curve of a control device [(ii) in Figure 4a] was measured using a scan rate of 0.02 V/s, as shown in Figure 4d. This device was prepared in a manner similar to the device (i) in Figure 4a, except without graphene on the bottom Cu electrode. It can be seen that the resistance of this device is overall lower. This is believed to be due to the Cu diffusion from the bottom electrode to ZnS during ZnS deposition (150 °C). Nonetheless, the absolute value of resistance should not be a concern because the switching behavior is more important for the comparison. In Figure 4d, a clear set process (arrow-1) is observed. After that, the device maintains itself in the LRS without any sign of reset. On the contrary, the device further switches to an even lower LRS (LLRS) at the voltage of −0.3 V (arrow-3) and returns to the original LRS when the voltage bounces back from −0.4 to −0.1 V (arrows 4 and 5). In the following cycles, the $I-V$ curve, which is not shown here, traces along the path of $\bar{2}2345$ in each cycle, where $\bar{2}$ represents the opposite direction of arrow 2. Despite a symmetric electrode pair of Cu–Cu, the $I-V$ curve of this device shows no symmetricity, which is counter-intuitive. However, after a careful analysis of the $I-V$ behavior, we believe that it actually attests the ion regulating role of graphene, which is explained as follows. Figure 4e schematically shows the evolution of CFs in this graphene-free device. Arrows 1 and 2 represent the normal formation of CFs when the top electrode under a positive bias voltage, just like the device (i) shown in Figure 4a does. When the top electrode is under a negative bias voltage, however, arrows 3 and 4 correspond to the formation of additional CFs from the opposite direction because of the absence of graphene. Contributed by the additional CF, the device goes from the LRS to the LLRS. Arrow 5 indicates the breaking of one of the conductive pathways, more likely being the additional CF because there is never a sign of turn-off to the HRS anywhere once the first CF is formed.

Besides CFs, the conducting path for resistive switching devices can also originate from a possible interface-type path.[35] In this type, the interface between electrodes and resistive switching layers is believed to play an important role on the charge transport behaviors through such ways as forming Ohmic contact, Schottky contact, interface dipoles, and so forth. For instance, the Schottky barrier effect has been used to interpret the rectification and hysteresis behaviors in $I-V$ characteristics and seems to be a legit explanation for resistive switching in a number of cases.[36,37] In the present work, a Schottky barrier, ΔE_1 = 0.75 eV, is expected to form at the interface between ZnS and the top Cu electrode, given the work function of Cu and electron affinity of ZnS.[22] However, the other interface formed by ZnS and graphene is more complex because the work function of graphene is dependent

DOI: 10.1021/acsami.7b18385
ACS Appl. Mater. Interfaces 2018, 10, 6730–6736

on the surroundings where graphene is placed.[38,39] Nonetheless, it can be reasonably assumed that ZnS and graphene also form a Schottky barrier with an unknown value of ΔE_2. As a result, the idealized energy diagram of the device (i) shown in Figure 4a can be sketched like in Figure S1. Here, by idealized, we mean that the interface dipoles or defects are ignored. Now that the interfaces are assumed to be of the Schottky type, a trial of using the Schottky barrier effect to interpret the resistive switching behaviors appears to be worthwhile. However, for any interface-type conducting path, the $I-V$ characteristics are highly dependent on the details, including the direction and magnitude, of the Schottky barrier heights which are unavailable. Thus, an attempt to interpret the $I-V$ characteristics using an interface-type conducting path in this work would be challenging.

While the central part of this work is to prove the concept of ion regulating using graphene, endurance and retention tests from the perspective of the device were also preliminarily studied on device (i) shown in Figure 4a. For the endurance test, 110 switching cycles between the HRS and the LRS were performed. The current at the HRS and the LRS was measured at 0.2 V. Figure 5a,b shows the measured current and its cumulative probability distribution, respectively. In spite of some fluctuation among cycles, the test indeed demonstrates the repeated reversibility of this resistive switching device. For the retention test, the current was measured at 0.15 V when the device was put in the HRS and the LRS, respectively. Figure 5c shows that the device can maintain in the LRS for up to ~3000 s before the instability shows up. Compared to other device-centering studies where tens of thousands of switching cycles in the endurance test and tens of thousands of seconds in the retention test were reported,[40,41] the tests in this work did not go that far because no device optimization was carried out. However, the device concept proposed in this work does hold several merits in other departments. First, the switching voltage is lower (less than 0.3 V) than usually reported (in several V).[31,42] Note, the electrolyte film was 200 nm in this study, which is thicker than the usual using of a couple tens of nm. This means that the switching actually occurs at a much lower magnitude in the sense of an electric field, which may be promising for ultralow power and ultrasensitive applications. Second, this ECM-based device avoids using Pt for the inert electrode and provides an alternative in graphene-buffered Cu. Compared to Pt, the combination of graphene and Cu is definitely a relief in cost for mass production.

CONCLUSIONS

In summary, an ECM memory using graphene to regulate Cu-ion migration is demonstrated with a vdWE Cu/ZnS(111)/graphene/Cu(111) heterojunction. The vdWE of ZnS on graphene is confirmed with an X-ray pole figure and Raman spectroscopy. The presence of graphene at the bottom Cu electrode is shown to effectively control the directionality in forming Cu CFs, which is evidenced by the highly asymmetrical $I-V$ characteristics measured from this memory and the direct comparison with the $I-V$ curve measured from a graphene-free memory. It is thus concluded that a graphene-covered Cu is sufficiently inert to serve as the inert electrode for ECM memories.

ASSOCIATED CONTENT

Supporting Information

The Supporting Information is available free of charge on the ACS Publications website at DOI: 10.1021/acsami.7b18385.

Schematic energy diagram of the Cu/ZnS/graphene/Cu ECM memory (PDF)

AUTHOR INFORMATION

Corresponding Author

*E-mail: sunx12@rpi.edu.

ORCID

Xin Sun: 0000-0001-5633-3371

Jian Shi: 0000-0003-2115-2225

Notes

The authors declare no competing financial interest.

ACKNOWLEDGMENTS

This work is supported by the NYSTAR Focus Center at RPI, C130117 and NSF Awards under DMR 1305293, CMMI 1550941, and CMMI 1635520. The authors wish to thank Micro and Nano Fabrication Clean Room (MNCR) staff at RPI for facilitating a part of the experimental work. The authors also wish to thank Prof. Nikhil Koratkar for offering the CVD furnace and Dr. Weiyu Xie for fruitful discussion.

REFERENCES

(1) Novoselov, K. S.; Fal'ko, V. I.; Colombo, L.; Gellert, P. R.; Schwab, M. G.; Kim, K. A roadmap for graphene. *Nature* **2012**, *490*, 192−200.

(2) Geim, A. K.; Grigorieva, I. V. Van der Waals heterostructures. *Nature* **2013**, *499*, 419−425.

(3) Kim, J.; Bayram, C.; Park, H.; Cheng, C.-W.; Dimitrakopoulos, C.; Ott, J. A.; Reuter, K. B.; Bedell, S. W.; Sadana, D. K. Principle of direct van der Waals epitaxy of single-crystalline films on epitaxial graphene. *Nat. Commun.* **2014**, *5*, 4836.

(4) Mohanty, D.; Xie, W.; Wang, Y.; Lu, Z.; Shi, J.; Zhang, S.; Wang, G.-C.; Lu, T.-M.; Bhat, I. B. van der Waals epitaxy of CdTe thin film on graphene. *Appl. Phys. Lett.* **2016**, *109*, 143109.

(5) Sun, X.; Lu, Z.; Xie, W.; Wang, Y.; Shi, J.; Zhang, S.; Washington, M. A.; Lu, T.-M. van der Waals epitaxy of CdS thin films on single-crystalline graphene. *Appl. Phys. Lett.* **2017**, *110*, 153104.

(6) Gopalan, C.; Ma, Y.; Gallo, T.; Wang, J.; Runnion, E.; Saenz, J.; Koushan, F.; Blanchard, P.; Hollmer, S. Demonstration of Conductive Bridging Random Access Memory (CBRAM) in logic CMOS process. *Solid-State Electron.* **2011**, *58*, 54−61.

(7) Morgan, K. A.; Fan, J.; Huang, R.; Zhong, L.; Gowers, R. P.; Jiang, L.; de Groot, C. H. Switching kinetics of SiC resistive memory for harsh environments. *AIP Adv.* **2015**, *5*, 077121.

(8) Valov, I.; Waser, R.; Jameson, J. R.; Kozicki, M. N. Electrochemical metallization memories—fundamentals, applications, prospects. *Nanotechnology* **2011**, *22*, 254003.

(9) Li, L.; Chen, X.; Wang, C.-H.; Cao, J.; Lee, S.; Tang, A.; Ahn, C.; Singha Roy, S.; Arnold, M. S.; Wong, H.-S. P. Vertical and Lateral Copper Transport through Graphene Layers. *ACS Nano* **2015**, *9*, 8361−8367.

(10) Mehta, R.; Chugh, S.; Chen, Z. Transfer-free multi-layer graphene as a diffusion barrier. *Nanoscale* **2017**, *9*, 1827−1833.

(11) Zhao, Y.; Liu, Z.; Sun, T.; Zhang, L.; Jie, W.; Wang, X.; Xie, Y.; Tsang, Y. H.; Long, H.; Chai, Y. Mass Transport Mechanism of Cu Species at the Metal/Dielectric Interfaces with a Graphene Barrier. *ACS Nano* **2014**, *8*, 12601−12611.

(12) Wang, H.; Xu, X.; Li, J.; Lin, L.; Sun, L.; Sun, X.; Zhao, S.; Tan, C.; Chen, C.; Dang, W.; Ren, H.; Zhang, J.; Deng, B.; Koh, A. L.; Liao, L.; Kang, N.; Chen, Y.; Xu, H.; Ding, F.; Liu, K.; Peng, H.; Liu, Z. Surface Monocrystallization of Copper Foil for Fast Growth of Large

Single-Crystal Graphene under Free Molecular Flow. *Adv. Mater.* **2016**, *28*, 8968−8974.
(13) Wu, W.; Jauregui, L. A.; Su, Z.; Liu, Z.; Bao, J.; Chen, Y. P.; Yu, Q. Growth of Single Crystal Graphene Arrays by Locally Controlling Nucleation on Polycrystalline Cu Using Chemical Vapor Deposition. *Adv. Mater.* **2011**, *23*, 4898−4903.
(14) Yang, H.; Heo, J.; Park, S.; Song, H. J.; Seo, D. H.; Byun, K.-E.; Kim, P.; Yoo, I.; Chung, H.-J.; Kim, K. Graphene Barristor, a Triode Device with a Gate-Controlled Schottky Barrier. *Science* **2012**, *336*, 1140−1143.
(15) Li, X.; Cai, W.; An, J.; Kim, S.; Nah, J.; Yang, D.; Piner, R.; Velamakanni, A.; Jung, I.; Tutuc, E.; Banerjee, S. K.; Colombo, L.; Ruoff, R. S. Large-Area Synthesis of High-Quality and Uniform Graphene Films on Copper Foils. *Science* **2009**, *324*, 1312−1314.
(16) Hu, Y.; Perello, D.; Yun, M.; Kwon, D.-H.; Kim, M. Variation of switching mechanism in TiO2 thin film resistive random access memory with Ag and graphene electrodes. *Microelectron. Eng.* **2013**, *104*, 42−47.
(17) Yao, J.; Lin, J.; Dai, Y.; Ruan, G.; Yan, Z.; Li, L.; Zhong, L.; Natelson, D.; Tour, J. M. Highly transparent nonvolatile resistive memory devices from silicon oxide and graphene. *Nat. Commun.* **2012**, *3*, 1101.
(18) Pirkle, A.; Chan, J.; Venugopal, A.; Hinojos, D.; Magnuson, C. W.; McDonnell, S.; Colombo, L.; Vogel, E. M.; Ruoff, R. S.; Wallace, R. M. The effect of chemical residues on the physical and electrical properties of chemical vapor deposited graphene transferred to SiO2. *Appl. Phys. Lett.* **2011**, *99*, 122108.
(19) Suk, J. W.; Kitt, A.; Magnuson, C. W.; Hao, Y.; Ahmed, S.; An, J.; Swan, A. K.; Goldberg, B. B.; Ruoff, R. S. Transfer of CVD-Grown Monolayer Graphene onto Arbitrary Substrates. *ACS Nano* **2011**, *5*, 6916−6924.
(20) Dlubak, B.; Kidambi, P. R.; Weatherup, R. S.; Hofmann, S.; Robertson, J. Substrate-assisted nucleation of ultra-thin dielectric layers on graphene by atomic layer deposition. *Appl. Phys. Lett.* **2012**, *100*, 173113.
(21) Koma, A. Van der Waals epitaxy—a new epitaxial growth method for a highly lattice-mismatched system. *Thin Solid Films* **1992**, *216*, 72−76.
(22) Zhuge, F.; Li, K.; Fu, B.; Zhang, H.; Li, J.; Chen, H.; Liang, L.; Gao, J.; Cao, H.; Liu, Z.; Luo, H. Mechanism for resistive switching in chalcogenide-based electrochemical metallization memory cells. *AIP Adv.* **2015**, *5*, 057125.
(23) Cardona, M.; Weinstein, M.; Wolff, G. A. Ultraviolet Reflection Spectrum of Cubic CdS. *Phys. Rev.* **1965**, *140*, A633−A637.
(24) Lu, Z.; Sun, X.; Xiang, Y.; Washington, M. A.; Wang, G.-C.; Lu, T.-M. Revealing the Crystalline Integrity of Wafer-Scale Graphene on SiO2/Si: An Azimuthal RHEED Approach. *ACS Appl. Mater. Interfaces* **2017**, *9*, 23081−23091.
(25) Sun, X.; Wang, Y.; Seewald, L. J.; Chen, Z.; Shi, J.; Washington, M. A.; Lu, T.-M. Decoupling interface effect on the phase stability of CdS thin films by van der Waals heteroepitaxy. *Appl. Phys. Lett.* **2017**, *110*, 041602.
(26) Robinson, Z. R.; Tyagi, P.; Mowll, T. R.; Ventrice, C. A.; Hannon, J. B. Argon-Assisted Growth of Epitaxial Graphene on Cu(111). *Phys. Rev. B: Condens. Matter Mater. Phys.* **2012**, *86*, 235413.
(27) Ferrari, A. C. Raman Spectroscopy of Graphene and Graphite: Disorder, Electron−Phonon Coupling, Doping and Nonadiabatic Effects. *Solid State Commun.* **2007**, *143*, 47−57.
(28) Ferrari, A. C.; Meyer, J. C.; Scardaci, V.; Casiraghi, C.; Lazzeri, M.; Mauri, F.; Piscanec, S.; Jiang, D.; Novoselov, K. S.; Roth, S.; Geim, A. K. Raman Spectrum of Graphene and Graphene Layers. *Phys. Rev. Lett.* **2006**, *97*, 187401.
(29) Costa, S. D.; Righi, A.; Fantini, C.; Hao, Y.; Magnuson, C.; Colombo, L.; Ruoff, R. S.; Pimenta, M. A. Resonant Raman Spectroscopy of Graphene Grown on Copper Substrates. *Solid State Commun.* **2012**, *152*, 1317−1320.
(30) Mooradian, A. Photoluminescence of Metals. *Phys. Rev. Lett.* **1969**, *22*, 185−187.
(31) Tsuruoka, T.; Terabe, K.; Hasegawa, T.; Aono, M. Forming and switching mechanisms of a cation-migration-based oxide resistive memory. *Nanotechnology* **2010**, *21*, 425205.
(32) Ielmini, D. Modeling the Universal Set/Reset Characteristics of Bipolar RRAM by Field- and Temperature-Driven Filament Growth. *IEEE Trans. Electron Devices* **2011**, *58*, 4309−4317.
(33) Ambrogio, S.; Balatti, S.; Choi, S.; Ielmini, D. Impact of the Mechanical Stress on Switching Characteristics of Electrochemical Resistive Memory. *Adv. Mater.* **2014**, *26*, 3885−3892.
(34) Bacaksız, E.; Dzhafarov, T. D.; Novruzov, V. D.; Öztürk, K.; Tomakin, M.; Küçükömeroğlu, T.; Altunbaş, M.; Yanmaz, E.; Abay, B. Copper diffusion in ZnS thin films. *Phys. Status Solidi A* **2004**, *201*, 2948−2952.
(35) Sawa, A. Resistive switching in transition metal oxides. *Mater. Today* **2008**, *11*, 28−36.
(36) Sawa, A.; Fujii, T.; Kawasaki, M.; Tokura, Y. Hysteretic current−voltage characteristics and resistance switching at a rectifying Ti/Pr0.7Ca0.3MnO3 interface. *Appl. Phys. Lett.* **2004**, *85*, 4073−4075.
(37) Fujii, T.; Kawasaki, M.; Sawa, A.; Akoh, H.; Kawazoe, Y.; Tokura, Y. Hysteretic current−voltage characteristics and resistance switching at an epitaxial oxide Schottky junction SrRuO3/SrTi0.99Nb0.01O3. *Appl. Phys. Lett.* **2005**, *86*, 012107.
(38) Song, S. M.; Park, J. K.; Sul, O. J.; Cho, B. J. Determination of Work Function of Graphene under a Metal Electrode and Its Role in Contact Resistance. *Nano Lett.* **2012**, *12*, 3887−3892.
(39) Yu, Y.-J.; Zhao, Y.; Ryu, S.; Brus, L. E.; Kim, K. S.; Kim, P. Tuning the Graphene Work Function by Electric Field Effect. *Nano Lett.* **2009**, *9*, 3430−3434.
(40) Balatti, S.; Ambrogio, S.; Wang, Z.; Sills, S.; Calderoni, A.; Ramaswamy, N.; Ielmini, D. Voltage-Controlled Cycling Endurance of HfOx-Based Resistive-Switching Memory. *IEEE Trans. Electron Devices* **2015**, *62*, 3365−3372.
(41) Yang, J. J.; Zhang, M.-X.; Strachan, J. P.; Miao, F.; Pickett, M. D.; Kelley, R. D.; Medeiros-Ribeiro, G.; Williams, R. S. High switching endurance in TaOx memristive devices. *Appl. Phys. Lett.* **2010**, *97*, 232102.
(42) Chang, W.-Y.; Lai, Y.-C.; Wu, T.-B.; Wang, S.-F.; Chen, F.; Tsai, M.-J. Unipolar resistive switching characteristics of ZnO thin films for nonvolatile memory applications. *Appl. Phys. Lett.* **2008**, *92*, 022110.

DOI: 10.1021/acsami.7b18385
ACS Appl. Mater. Interfaces 2018, 10, 6730−6736